IEEE Open Journal of Vehicular Technology

Received 31 March 2023; accepted 24 June 2023. Date of publication 5 July 2023;
date of current version 4 August 2023. The review of this article was coordinated by Editor Lina Bariah.

Digital Object Identifier 10.1109/OJVT.2023.3292183

A Channel Loss Model for THz Networks From 100–600 GHz Considering Both Molecular and Water Vapor Continuum Absorptions

RAFAEL V. T. DA NOBREGA [1,2], THIAGO R. RADDO [3], ANTONIO JURADO-NAVAS [3], MURILO B. LOIOLA [2], ANDERSON L. SANCHES [2], AND MEROUANE DEBBAH [4] (Fellow, IEEE)

[1]Academic Area of Electrical Engineering, Federal Institute of Minas Gerais, Formiga 35570-000, Brazil
[2]Engineering, Modeling, and Applied Social Sciences Center, Federal University of ABC, Santo Andre 09210-580, Brazil
[3]Communication and Signal Processing Laboratory, Telecommunication Research Institute (TELMA), University of Malaga, 29016 Malaga, Spain
[4]Khalifa University of Science and Technology, Abu Dhabi 127788, UAE

CORRESPONDING AUTHOR: ANTONIO JURADO-NAVAS (e-mail: navas@ic.uma.es).

This work was supported in part by the University of Malaga, Spain, in part by the Federal institute of Minas Gerais (IFMG), in part by the Federal University of ABC (UFABC), Brazil, and in part by the Telecommunication Research Institute, Spain.

ABSTRACT 6G networks are expected to use the terahertz (THz) frequency spectrum in some way. However, relatively little is known about the transmission channel in this part of the spectrum. In this article, we propose a novel and accurate channel loss model that considers both molecular and water vapor continuum absorptions for THz networks based on the frequency range between 100 GHz and 600 GHz. The proposed channel model assumes that the atmospheric absorption is accurately accounted for by the molecular absorption coefficient and the water vapor continuum absorption coefficient. The new model is based on equations developed to accurately match the channel response given by a spectroscopic database. This makes the channel model robust and useful for evaluating the performance of THz networks. The model is validated against a spectroscopic database defined as a benchmark. The performance of the new channel loss model is evaluated against different models, including several error metrics. Numerical results show the new channel model is as accurate as the spectroscopic database by correctly reproducing the provided experimental dataset. Therefore, the proposed channel model is a reliable, robust and simple tool that can be successfully used to carry out performance evaluation of THz networks with accuracy.

INDEX TERMS Absorption loss, channel model, THz, 6G, water vapor continuum absorption.

I. INTRODUCTION

Over the past few years, there has been a growing demand for broadband services offered by mobile networks, taking data traffic volumes to unprecedented levels [1], [2]. Mobile networks are expected to handle an increase in global traffic volume that is currently doubling every two years [3]. Importantly, this constant raising in broadband services demand and data traffic generation will pose challenges on power consumption. Regardless of the sector, the latter is becoming a paramount concern mainly due to both climate change and limitation of renewable energy resources. The current levels of greenhouse gas emissions and their environmental impact are unsustainable and pose a real challenge to industries, even putting in risk their capacity to achieve net zero emission by 2050 [3]. One eventual way to reduce the gas emissions and environmental impact, is dematerialization. The telecom industry has the potential to lessen the need for material usage by substituting physical products with digital ones. Dematerialization [3], which leads to reduced consumption of natural resources, can be achieved for example via VR/AR, holograms, and metaverse. Holograms not only can enable many applications, but also allow for a true virtual representation of complex entities of the physical world, helping reduce the total quantity of exemplars of several goods. This would potentially lead to a successful dematerialization and consequently environmental impact reduction. Notwithstanding, holograms, VR/AR, and metaverse [4], [5] are broadband applications requiring larger bandwidth and higher data rates

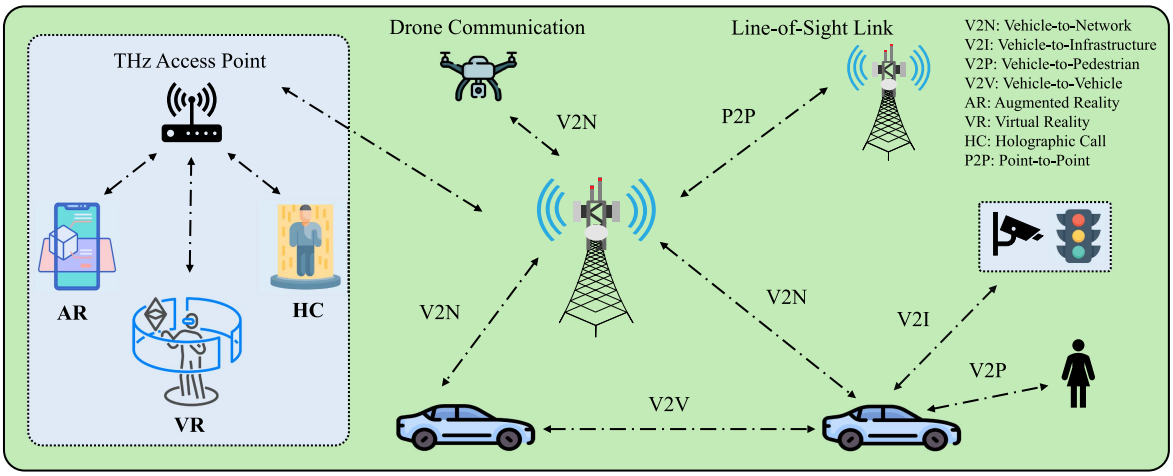

FIGURE 1. Illustration of a THz network supporting potential applications based on V2X, VR/AR, and holograms.

(as well as lower latency) than offered by current networking solutions. In fact, these emerging applications will most likely not be fully satisfied by current fifth-generation (5G) technologies [6], but, instead, will require support to ultra-high data rates up to terabits per second (Tb/s) and highly accurate positioning [7]. Higher frequencies within the terahertz (THz) region is envisioned as a key technology to satisfy this demand by alleviating the spectrum scarcity and capacity limitations of current mobile systems. Following this trend, Tb/s wireless links will become a reality within the upcoming years.

As societal needs evolves, next-generation networks such as 6G will require higher frequencies to satisfactorily serve these demanding applications. Accordingly, 6G networks based on the THz spectrum will provide a significant improvement in bandwidth availability, data rates, and full symmetric duplex operation [8]. Eventually, in future systems, both uplink and downlink will have similar capabilities, especially in terms of bandwidth and data rates. In this way, the THz bands can grant 6G networks the feasibility to support wider bandwidth and higher data-rates. Not only can this be the key to supporting future data traffic demands, but also a way to enable dematerialization. 6G networks based on THz bands can further enable different networking scenarios like for example vehicle-to-everything (V2X) communications [9], [10], environment virtualization [11], and holograms [12], to name but a few. Such a scenario is illustrated in Fig. 1, where 6G-based THz networks enable a new range of applications and several devices are simultaneously served by multiple access points through multi-point transmissions.

6G networks may use part of the spectrum defined between 0.1–10 THz. While the frequency regions immediately below and above this range (the microwaves and the far infrared) have been extensively investigated, this is still one of the least explored frequency bands for communication, with several open challenges. The THz Interest Group IEEE 802.15 [13] responsible for standardization of THz communications was created and the IEEE 802.15.3d-2017 became the world's first wireless standard at 300 GHz [14]. Despite standardization efforts, there are many open challenges for leveraging THz communications and its capabilities [15], [16], [17]. Among them, the channel propagation model renders THz-based networks to be misleading in its performance and future potential. Therefore, a new channel model for 6G/THz networks is addressed here. A reliable THz channel loss model is key for helping developing as well as evaluating mobile systems. In this way, a reliable and accurate channel model must include the molecular absorption loss as well as the water vapor continuum absorption loss [18], [19].

The molecular absorption loss can be obtained via two different ways. The first way is the line-by-line functions which account for the molecular attenuation based on the HITRAN (high-resolution transmission) spectroscopic database in combination with the Van Vleck-Weisskopf (VVW) line shape functions [18], [20], [21]. For example, in the ITU-R P.676-13 Recommendation [22] the atmospheric attenuation in the range between 1 and 1000 GHz is defined. Such a recommendation is based on a numerical method that calculates the individual summation of spectral lines (i.e. line-by-line calculation) by using 553 spectroscopic data points from the HITRAN database in combination with the full Lorentz line shape functions in order to finally be capable of evaluating the atmospheric attenuation. The usage of the spectroscopic data along with line-by-line calculations not only adds complexity to the evaluation, rendering the same an arduous procedure, but also is an approximate method which may not provide accurate results.

In contrast, the second way to address the molecular absorption loss is via closed-form expressions [23], [24], [25], [26]. Accordingly, a set of equations to evaluating the molecular attenuation considering water vapor is reported in the ITU-R P.676-10 Recommendation [23]. This model is

based on full Lorentz line shape functions with the coefficients fitted to experimental measurements [27], [28], but with low accuracy and limited for the 1–350 GHz frequency range.

Furthermore, a simplified channel model for the frequency range of 275–400 GHz is reported in [24]. Such a model is based on polynomials and an equalization factor for fitting purposes along with Van-Vleck Huber line shape functions using the parameters from the HITRAN database. This simplified model was subsequently extended in order to cover the frequency range of 200–450 GHz in [25]. Later on, the 200–450 GHz channel loss model was further developed by including new polynomials to cover the frequency range between 100 and 450 GHz in [26]. Despite being capable of covering the D-band, such a channel loss model is not accurate for its entire frequency range and has high average error. Lastly, the water vapor continuum attenuation, which contributes to the atmospheric attenuation, was not taken into account by the model [26].

By its turn, the water vapor continuum attenuation can be calculated via empirical equations fitted for the THz region [19], [29], [30], [31], [32]. The contribution of the water vapor continuum absorption in the evaluation of the atmospheric absorption coefficient is highlighted in [30]. The absence of the continuum spectrum can lead to discrepancies around hundreds of dB for transmission distances over a kilometer. The attenuation of the water vapor continuum absorption up to 1 THz is investigated in [32]. The latter defines the empirical coefficient parameters that describe the most accurate attenuation due to the water vapor continuum absorption spectrum.

Within this context, in this article a new and accurate channel loss model for the frequency range between 100 and 600 GHz is proposed. The new channel model developed here accounts for the total atmospheric absorption by taking into account both the molecular absorption coefficient and the water vapor continuum absorption coefficient. This allows, for the first time, to the best of our knowledge, the THz transmission channel loss to be accurately accounted for. The newly developed channel model is based on closed-form equations given by absorption line shape functions and a fitting parameter. The new model is validated against the HITRAN database, which is defined as a benchmark. The mean absolute error (MAE), root mean squared error (RMSE), mean absolute percentage error (MAPE), maximum absolute error, and adjusted R-squared for the proposed channel loss model are calculated and analyzed. Moreover, the performance of the proposed channel loss model is evaluated against many different models. Numerical results show that the new channel model matches the performance behaviour of experimental dataset from the HITRAN spectroscopic database for the designed frequency range. This renders the proposed channel model to be an accurate and reliable tool for performance evaluation of THz networks based on 100 - 600 GHz. Lastly, the newly developed accurate model enables the evaluation of key figures-of-merit (that are dependent on the channel losses) in THz networks such as free-space path-loss (FSPL), signal-noise-rate (SNR), and bit error rate (BER), as analyzed here.

II. MATHEMATICAL FRAMEWORK

Communication systems are expected to transmit information from one point to another. They are normally made up of transmitters, a channel, and receivers. Briefly, at the transmitter the modulation of signals occurs, and then they are sent through a channel to the receiver. Two features in a communication system can be highlighted: the transmitted power and the channel bandwidth [33], [34]. The transmitted power defines the SNR, and depends on the transmitter's design. On the other hand, the channel bandwidth is defined as the frequency range allocated for signal transmission, and can be obtained by modeling the channel.

In addition, the THz band is formed by multiple absorption lines that are unique for each molecule present in the atmosphere. The energy associated with the change of quantum levels determines the frequency of the absorption line, and this frequency can be altered by some environmental factors, such as the change of temperature, pressure, and the quantity of water vapor in the atmosphere [18].

Thus, the THz channel can be modeled as [35], [36]

$$y = hx + n, \tag{1}$$

where x is the transmitted signal, y is the received signal, n is the noise, and h is the channel state given by

$$h = h_p h_{atm}, \tag{2}$$

where h_p and h_{atm} represent the propagation gain and the atmospheric absorption fading. According to the Friis equation, h_p in the free space can be given by [34]

$$h_p = \frac{c}{4\pi df}\sqrt{G_{Tx}G_{Rx}}, \tag{3}$$

with c, G_{Tx}, G_{Rx}, d, and f denote the speed of light, the transmitter antenna gain, the receiver antenna gain, the transmission distance, and the THz wave frequency, respectively. Based on the Beer-Lambert Law, h_{atm} is given by [18]

$$h_{atm} = e^{-\frac{1}{2}k(f)d} = e^{-\frac{1}{2}(k_a(f)+k_c(f))d}, \tag{4}$$

where $k(f)$ is the total absorption coefficient of the THz channel, which is composed of the sum of the molecular absorption coefficient, $k_a(f)$, and the water vapor continuum absorption coefficient, $k_c(f)$ [18], [19]. Next, the channel noise power is an important system metric, and it can be calculated as follows [18]

$$P_n(f,d) = k_B \int_{\Delta f} T_{noise}(f,d)df, \tag{5}$$

where k_B is the Boltzmann constant, Δf is the channel available bandwidth and T_{noise} is the channel noise temperature which is given by

$$T_{noise} = T_{sys} + T_{atm} + T_{other}, \tag{6}$$

with T_{sys} is the system electronic noise temperature, T_{atm} is the atmospheric absorption noise, and T_{other} considers any additional noise source. Thus, T_{sys} is given by

$$T_{sys} = T\,(\mathrm{NF} - 1)\,, \tag{7}$$

where NF is the noise factor, whose value in dB represents the system noise figure, and T is the system temperature. T_{atm} is obtained by

$$T_{atm} = T\left(1 - \exp\left(-k(f)d\right)\right) = T\left(1 - \tau(f,d)\right), \tag{8}$$

with $\tau(f,d)$ is the channel transmittance in the medium, and it can be related to the transmitter (P_{Tx}) and receiver (P_{Rx}) powers as

$$\tau(f,d) = \exp\left(-k(f)d\right) = \frac{P_{Rx}}{P_{Tx}}, \tag{9}$$

emphasizing that $k(f) = k_a(f) + k_c(f)$.

For the communication systems considered here, it is assumed that $T_{sys} + T_{atm} \gg T_{other}$, and then, (6) can be rewritten as

$$T_{noise}(f,d) = T_{sys} + T_{atm} = T\left(\mathrm{NF} - \tau(f,d)\right), \tag{10}$$

and from (10), we can determine the channel noise power given by (5). It is worth mentioning that the phase noise of the signal is adequately compensated by advanced digital signal processing techniques at the receiver side [37]. In this way, from (3) and (4), one can obtain the total line-of-sight (LOS) path loss (PL) of a THz wave propagating in the atmosphere as [33], [36]

$$\mathrm{PL\,[dB]} = 20\log_{10}\left(\frac{4\pi df}{c}\right) + 10k(f)d\log_{10}e, \tag{11}$$

where e is Euler's number. The system transmits on-off pulses employing on-off keying (OOK) modulation. Complex modulation formats such as pulse-amplitude modulation [38] will be considered as future work. Lastly, the SNR of the system can be calculated as

$$\mathrm{SNR}(f,d) = \left(\frac{c}{4\pi df}\right)^2 \frac{P_{Tx}G_{Tx}G_{Rx}\tau(f,d)}{k_B\int_{\Delta f} T\left(\mathrm{NF} - \tau(f,d)\right)df}, \tag{12}$$

and the BER of the system is given by [39]

$$\mathrm{BER}(f,d) = \frac{1}{2}\mathrm{erfc}\left(\frac{1}{2}\sqrt{\frac{\mathrm{SNR}(f,d)}{2}}\right), \tag{13}$$

where erfc (x) is the complementary error function. Next, the methods for calculating the molecular absorption and water vapor continuum absorption coefficients are presented.

A. MOLECULAR ABSORPTION COEFFICIENT

The molecular absorption coefficient, $k_a(f)$, can be obtained via two different approaches, namely, the numerical and simplified models. First, the numerical modeling is based on radiative transfer theory with information supplied by the HITRAN database [18], [21]. Thus, $k_a(f)$ can be obtained by the following expression [18]

$$k_a^{num}(f) = \sum_{i,g} k_a^{i,g} = \sum_{i,g} \frac{N_A}{R}\frac{T_{STP}}{p_0}\left(\frac{p}{T}\right)^2 q^{i,g}S^{i,g}F^{i,g}(f), \tag{14}$$

where $k_a^{i,g}$ is the individual absorption coefficient for the isotopologue i of gas g, N_A is the Avogadro constant, R is the universal gas constant, p and T are the system pressure and temperature, respectively, p_0 and T_{STP} are the standard-pressure-temperature values. In addition, $q^{i,g}$, $S^{i,g}$, and $F^{i,g}(f)$ are the mixing ratio, spectral line intensity, and line shape functions for the isotopologue i of gas g, respectively. The quantities $S^{i,g}$ and $F^{i,g}(f)$ are obtained from the HITRAN database [21]. More details for obtaining $k_a(f)$ numerically can be found in [18], [40].

Next, the molecular absorption coefficient can be alternatively obtained via simplified models [26]. Accordingly, the model presented in [26] is based on fitted equations with numerical results determined from the radiative transfer theory in combination with the HITRAN spectroscopic database, but for the frequency range of 100 to 450 GHz. The coefficients of the equations depend on the temperature, pressure (fixed), and relative humidity (RH) of varied water vapor in the atmosphere. Furthermore, the parametric model is characterized by the molecular absorption coefficients y_j on absorption lines j. The simplified molecular absorption coefficient is given by [26]

$$k_a^{simpl}(f) = \sum_{j=6} y_j(f,\mu) + g(f,\mu), \tag{15}$$

with f is the frequency of interest, $g(f,\mu)$ is a fitting equation, and μ is the water vapor mixing ratio that depends directly on RH [26], and it is given by

$$\mu = \frac{\mathrm{RH}(\%)}{100}\frac{p_s(T,p)}{p}, \tag{16}$$

where RH(%) is the relative humidity given in percentage and p_s is the saturated water vapor partial pressure, and is described by Buck's equation [26]

$$p_s = 6.1121\left(1.0007 + 3.46\times10^{-6}p\right)\exp\left(\frac{17.502\,T}{240.97 + T}\right), \tag{17}$$

where the pressure p is given in hectopascals and T is given in degree Celsius. Subsequently, we carry on the development of the channel model but assuming an accurate molecular absorption coefficient and the frequency range of 100 to 600 GHz.

1) NOVEL PROPOSED CHANNEL MODEL

A new channel loss model is developed here considering polynomials for the absorption coefficient as well as a frequency range of 100–600 GHz. To do so, new equations describing the absorption peaks are developed. In addition, a fit equation parameter is also developed and included in the $g(f,\mu)$ in order to accurately fit (the new model behaviour) with

(experimental) spectroscopic database. Hence, the molecular absorption coefficient is calculated as

$$k_a^{ext}(f) = \sum_{j=10} y_j(f,\mu) + g(f,\mu), \tag{18}$$

and, the polynomial equations representing the strong absorption lines in the 100 to 450 GHz range are [26]

$$y_1(f,\mu) = \frac{A(\mu)}{B(\mu) + \left(\frac{f}{100c} - p_1\right)^2}, \tag{19}$$

$$y_2(f,\mu) = \frac{C(\mu)}{D(\mu) + \left(\frac{f}{100c} - p_2\right)^2}, \tag{20}$$

$$y_3(f,\mu) = \frac{E(\mu)}{F(\mu) + \left(\frac{f}{100c} - p_3\right)^2}, \tag{21}$$

$$y_4(f,\mu) = \frac{G(\mu)}{H(\mu) + \left(\frac{f}{100c} - p_4\right)^2}. \tag{22}$$

Then, without loss of generality, we new develop here the resonant absorption lines for the center frequencies at 425, 475, 487, and 557 GHz as follows

$$y_5(f,\mu) = I(\mu) + \frac{J(\mu)}{4(f-f_5)^2 + w_5(\mu)^2} + K(\mu)\exp\left[-\alpha\left(\frac{f-f_5}{w_5(\mu)}\right)^2\right], \tag{23}$$

$$y_6(f,\mu) = \frac{L(\mu)}{M(\mu) + \left(\frac{f}{100c} - p_6\right)^2}, \tag{24}$$

$$y_7(f,\mu) = \frac{N(\mu)}{O(\mu) + \left(\frac{f}{100c} - p_7\right)^2}, \tag{25}$$

$$y_8(f,\mu) = \frac{P(\mu)}{Q(\mu) + \left(\frac{f}{100c} - p_8\right)^2}, \tag{26}$$

$$y_9(f,\mu) = R(\mu) + \frac{S(\mu)}{4(f-f_9(\mu))^2 + w_9(\mu)^2} + T(\mu)\exp\left[-\alpha\left(\frac{f-f_9(\mu)}{w_9(\mu)}\right)^2\right], \tag{27}$$

$$y_{10}(f,\mu) = U(\mu) + \frac{V(\mu)}{4(f-f_{10}(\mu))^2 + w_{10}(\mu)^2}, \tag{28}$$

whose coefficients are given by

$$A(\mu) = \left(7.35165\times10^{-6} - 7.32078\times10^{-6}\mu - 3.08766\times10^{-8}\mu^2\right)/\left(1.04837 - 3.70531\mu\right), \tag{29}$$

$$B(\mu) = \left(-2.09\times10^{-4}(1-\mu) + 5\times10^{-2}\right)^2, \tag{30}$$

$$C(\mu) = \frac{6.1215\times10^{-3}\mu + 2.59875\times10^{-2}\mu^2}{0.98494 - 1.04473\mu}, \tag{31}$$

$$D(\mu) = \left(0.4241\mu + 9.98\times10^{-2}\right)^2, \tag{32}$$

$$E(\mu) = 6.82059\times10^{-3}\mu + 3.96559\times10^{-2}\mu^2 + 4.19415\times10^{-2}\mu^3, \tag{33}$$

$$F(\mu) = 9.55486\times10^{-3} + 8.462\times10^{-2}\mu + 0.18735\mu^2, \tag{34}$$

$$G(\mu) = \left[\frac{2.053\mu\,(0.1717\mu + 0.0306)}{1.01827 - 0.64956\mu}\right] \times \left(0.98825 + 8.37\times10^{-3}\exp\left(57.67013\mu\right)\right), \tag{35}$$

$$H(\mu) = 9.41068\times10^{-3} + 0.10564\mu + 0.29648\mu^2, \tag{36}$$

$$w_5(\mu) = 3.35001\times10^{9} + 2.53134\times10^{10}\mu, \tag{37}$$

$$I(\mu) = 5.67576\times10^{-5} + 0.22289\mu, \tag{38}$$

$$J(\mu) = \frac{2w_5(\mu)}{\pi}\left(3.4759\times10^{6} + 1.15834\times10^{8}\mu + 4.15911\times10^{8}\mu^2 - 7.10939\times10^{9}\mu^3\right) \times \left(7.43613 + 1.41038\exp\left(-99.7009\mu\right)\right), \tag{39}$$

$$K(\mu) = \sqrt{\frac{\alpha}{\pi\, w_5(\mu)^2}}\left(1.40996\times10^{4} - 2.69183\times10^{7}\mu - 4.15911\times10^{8}\mu^2 + 7.10939\times10^{9}\mu^3\right) \times \left(7.43613 + 1.41038\exp\left(-99.7009\mu\right)\right), \tag{40}$$

$$L(\mu) = 0.177\mu\,(0.0832\mu + 0.0213), \tag{41}$$

$$M(\mu) = (0.2615\mu + 0.0668)^2, \tag{42}$$

$$N(\mu) = 2.146\mu\,(0.1206\mu + 0.0277), \tag{43}$$

$$O(\mu) = (0.3789\mu + 0.0871)^2, \tag{44}$$

$$P(\mu) = \frac{9.695\times10^{-3}\mu + 4.221\times10^{-2}\mu^2}{1.09281 - 1.94936\mu}, \tag{45}$$

$$Q(\mu) = 7.58641\times10^{-3} + 6.60044\times10^{-2}\mu + 0.14356\mu^2, \tag{46}$$

$$f_9(\mu) = 4.87286\times10^{11} + 4.08547\times10^{10}\mu - 5.08079\times10^{11}\mu^2, \tag{47}$$

$$w_9(\mu) = 3.40115\times10^{9} + 4.56867\times10^{10}\mu - 5.85855\times10^{11}\mu^2, \tag{48}$$

$$R(\mu) = -2.09394\times10^{-4} + 0.84409\mu, \tag{49}$$

$$S(\mu) = \frac{2w_9(\mu)}{\pi}\Big(1.72001 \times 10^7 - 3.96597 \times 10^8\mu - 2.13925 \times 10^{10}\mu^2 + 5.23041 \times 10^{11}\mu^3 + 9.91933 \times 10^{11}\mu^4\Big), \quad (50)$$

$$T(\mu) = \sqrt{\frac{\alpha}{\pi w_9(\mu)^2}}\Big(-9.00089 \times 10^5 + 1.00072 \times 10^9\mu + 2.2412 \times 10^{10}\mu^2 - 5.2304 \times 10^{11}\mu^3 - 9.9193 \times 10^{11}\mu^4\Big), \quad (51)$$

$$f_{10}(\mu) = 5.56983 \times 10^{11} + 1.5944 \times 10^8\mu, \quad (52)$$

$$w_{10}(\mu) = 6.23187 \times 10^9 + 1.46195 \times 10^{10}\mu, \quad (53)$$

$$U(\mu) = 7.20497 \times 10^{-11} + 7.545 \times 10^{-8}\mu, \quad (54)$$

$$V(\mu) = \frac{2w_{10}(\mu)}{\pi}\Big(-2.79148 \times 10^7 + 3.79879 \times 10^{12}\mu + 3.57152 \times 10^{10}\mu^2\Big). \quad (55)$$

Then, without loss of generality, the fitting equation $g(f, \mu)$ can be developed as follows

$$g(f, \mu) = \frac{\mu}{1.391 \times 10^{-2}}\left(\theta_{adj} + 10^{-112}f^9\right) - 1.10086\mu + 2.91788 \times 10^{-4}, \quad (56)$$

with the following constant values $\alpha = 2.77256$, $f_5 = 424.8 \times 10^9$ Hz, $p_1 = 3.96274$ cm^{-1}, $p_2 = 6.11423$ cm^{-1}, $p_3 = 10.8475$ cm^{-1}, $p_4 = 12.6829$ cm^{-1}, $p_6 = 14.65$ cm^{-1}, $p_7 = 14.9436$ cm^{-1}, $p_8 = 15.835$ cm^{-1}, and θ_{adj} is the optimization parameter used to improve the fitting of the proposed channel model. The coefficients of $A(\mu)$, $C(\mu)$, $E(\mu)$, $F(\mu)$, $G(\mu)$ and $H(\mu)$, are new and developed here. They now represent the correct amplitudes for RH values varying from 10%, 30%, 50%, 70% and 90%.

Note that the resonance absorption lines y_5, y_9 and y_{10}, in (23), (27) and (28), respectively, are based on the pseudo-Voigt peak function [41]. Such a function is defined by the convolution of the Gaussian and Lorentzian functions, and it is generally used to obtain experimental spectral line shapes [41]. In contrast, the coefficients from (23), (27) and (28) are obtained by the help of the HITRAN database and VVW functions along with fitting procedure. The fitting procedure is carried out to determine in an accurate way the new expressions of the absorption line coefficients according to the numerical model from [18], [21], [40].

Finally, the (56) is developed via the fitting procedure described earlier. Hence, (56) depends on the optimization parameter, θ_{adj}, which has an optimal value for each frequency band in the 100–600 GHz range. Then, once the optimized θ_{adj} is obtained, the mean absolute error (MAE) can be minimized. Next, we address the formalism to obtain the water vapor continuum absorption coefficient.

B. WATER VAPOR CONTINUUM ABSORPTION COEFFICIENT

The water vapor is one of the main elements responsible for the atmospheric attenuation of electromagnetic waves propagating in the THz band [19], [29], [30], [31], [32]. There are two components of atmospheric attenuation related to water vapor which are resonant absorption lines and continuum absorption [19]. The contribution of the water vapor absorption lines is accounted for in (18). The continuum absorption coefficient rises quadratically as the frequency increases and decreases inversely as the temperature increases in the THz region (up to ~3 THz) [19], [29], [30], [31], [32]. Therefore, according to [19], [31], the water vapor continuum absorption coefficient can be expressed as

$$k_c(f) = f^2\left(C_W^0\theta^{n_W+3}P_W^2 + C_A^0\theta^{n_A+3}P_AP_W\right) = f^2\left(C_WP_W^2 + C_AP_AP_W\right), \quad (57)$$

where f is the frequency in GHz, P_W and P_A are the partial pressures of the water vapor and foreign gases in the atmosphere, respectively, C_W^0 and C_A^0 are the water vapor and foreign-continuum parameters at 300 K, in units of (dB/km)/(hPa GHz)^2, respectively. $\theta = 300/T$ is the dimensionless temperature factor, and T is the system temperature in K. n_W and n_A are the temperature exponents. And then, $C_W = C_W^0\theta^{n_W+3}$ and $C_A = C_A^0\theta^{n_A+3}$ are the water vapor and foreign-continuum parameters as a function of temperature, respectively. As the water vapor continuum absorption coefficient is usually obtained empirically, the values of the parameters are given by experimental works, such as [19], [29], [30], [31], [32]. For the channel loss model proposed herein, we consider the empirical parameters from [29], which gives $C_W = 4.39 \times 10^{-8}$ (dB/km)/(hPa GHz)^2 and $C_A = 4 \times 10^{-9}$ (dB/km)/(hPa GHz)^2 for the room temperature.

Concerning the partial pressures P_W and P_A, they are determined as follows

$$P_W = \mu p_0, \text{ and } P_A = (1-\mu)\,p_0, \quad (58)$$

respectively, recalling that μ is the water vapor mixing ratio and p_0 is the standard pressure given in hPa. From the parameters P_W, P_A, C_A and C_W, and using (57), the water vapor continuum absorption coefficient can be calculated. Lastly, the total atmospheric absorption coefficient, $k(f)$, is composed of the sum of the molecular absorption coefficient, $k_a(f)$ given by (18), and the water vapor continuum absorption coefficient, $k_c(f)$ given by (57), for a specified temperature value.

III. RESULTS AND DISCUSSION

The thoroughly described channel loss model is now applied for the performance evaluation of THz networks based on 100–600 GHz. Its performance and accuracy is assessed against several models.

A. NUMERICAL VALIDATION OF THE MOLECULAR ABSORPTION COEFFICIENT

The numerical model based on the Radiative Transfer Theory, using the VVW line shapes and the spectroscopic data

obtained from the HITRAN database [18], [21], [40] is considered here as the benchmark. Then, the contributions to the molecular absorption of each isotopologue i of each gas g present in the atmosphere is calculated. Afterwards, the molecular absorption coefficient of the THz channel is determined by (14). Subsequently, by using the numerical approach, the molecular absorption coefficients of each type of molecule available in the atmosphere is calculated. To do so, the percentages of molecules in the atmosphere are considered as: $N_2 = 78.084\%$, $O_2 = 20.946\%$ and $CO_2 = 0.0417\%$. Furthermore, the atmospheric pressure of 1 atm (1.01325×10^3 hPa), temperature equal to 298 K (25 °C), and RH ranging from 10% to 90% (with a 20% step) are considered.

The numerical molecular absorption coefficient results (VVW + HITRAN) for RH = 10% and 90%, in the 100 to 450 GHz range, are shown in Fig. 2(a) and (b), respectively. It can be noted from Fig. 2 that for higher RH values, the larger the molecular absorption coefficients are, which suggests that water molecules are responsible for the major absorption loss in the atmosphere. It can also be seen from Fig. 2 that there are well-defined peaks at some frequencies. These are the resonance peaks given by the line-by-line absorption model [18], [21], [40]. However, between two adjacent peaks there are some lower values of the absorption coefficient. This region between adjacent peaks can be regarded as potential transmission windows for THz wireless communication systems.

Moreover, Fig. 2 shows the performance comparison among the channel model given by [26], the numerical ITU-R model referred here as Full-ITU-R [22], the numerical VVW + HITRAN model (that is considered as benchmark) [18], [21], and the new proposed model. One can observe from Fig. 2(a), that the new proposed model (black lines) is the only one to converge and complete agree/overlap with the benchmark model (red lines). The performance estimation difference, among the channel models, becomes even more evident for the strong resonance peaks with center frequencies at 119 GHz and 425 GHz, where the remaining channel models clearly cannot reproduce the peaks according to the bechmark. Moreover one can further notice that the regions between peaks 1 and 2 (119–183 GHz), 2 and 3 (183–325 GHz), and 3 and 4 (325–380 GHz) show some divergence between the absorption lines in these transmission windows, for the model from [26], misleading the performance of the network. For example, under 119 GHz and RH = 10%, while the proposed model is as accurate as the benchmark, the models left underestimate the molecular absorption losses in an order of magnitude. Furthermore, analyzing the top inset in Fig. 2(a), the D-band (110–170 GHz) is highlighted, and it can be infered that the peak around 119 GHz for the benchmark and proposed models have 13 dB/km, whereas the models from [26] and Full ITU-R have 1.4 dB/km only. This difference among models, undestimates the network performance in an order of magnitude, which may be unaccetable in THz systems where signal power transmission is key for the smooth network operation. Also, the range from 400 to 450 GHz is

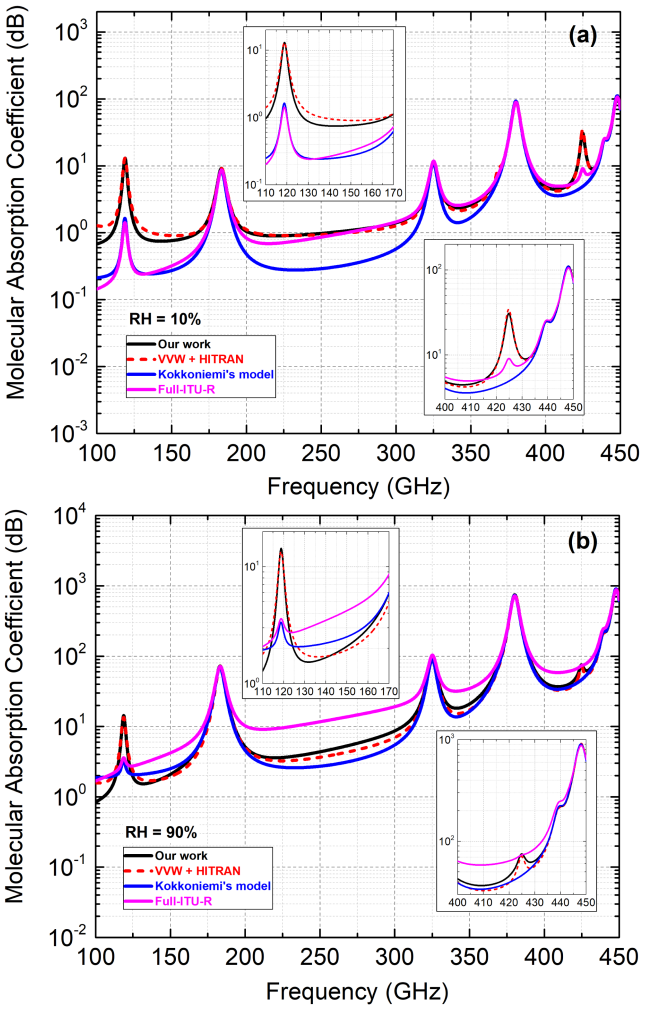

FIGURE 2. Comparison between the molecular absorption coefficient as a function of frequency from 100 to 450 GHz obtained by the different models for transmission distance of one kilometer, and different RH levels: (a) 10% and (b) 90%. In both figures: the top inset shows the D-band (110–170 GHz) in evidence, and the bottom inset shows the 400 to 450 GHz band.

highlighted in the bottom inset from Fig. 2(a), once again, it can be realized that for the peak around 425 GHz, the proposed and benchmark models have 30.3 dB/km, whereas the Full-ITU-R model has 9.1 dB/km, and [26] simply misses the peak.

The molecular absorption coefficient versus the frequency is plotted in Fig. 2(b) for RH = 90%. In such a figure, one can note that the both benchmark (red) and our proposed channel model (black) peaks at 425 GHz, whereas the remaining model (blue) and ITU-R (pink) are smoothly throughout the region. As a result, the performance of the THz system is hindered. In contrast, it can be further noted from Fig. 2(b) that all models peak at 119 GHz, while our model (black) excellently agrees with the benchmark (red) instead, the remaining model (blue) and ITU-R (pink) peak shorter, resulting in a short tail and consequently underestimating the channel loss

estimation for a wider range of frequencies. Surprisingly, the ITU-R model (pink curve) has a heavy tail than do the all remaining models for the entire frequency range, but even more substantial in the frequency window between peaks 2 and 3 (183–325 GHz), as can be seen in Fig. 2(b). As a consequence, the ITU-R model predicts higher molecular absorption losses in the THz channel than one would actually expect. To circumvent this issue, someone should eventually use the experimental/spectroscopic database solution, or the channel loss model proposed in this work. Additionally, in such top inset from Fig. 2(b), on one hand, both benchmark and proposed model have around 14.1 dB/km at 119 GHz, and on the other hand, the Full-ITU-R (pink) and remaining (blue) models have around 3.6 dB/km at 119 GHz. Lastly, in such bottom inset from Fig. 2(b), while the proposed and benchmark models have 75.2 dB/km at 425 GHz, the previous model (blue) does not peak, and has an absorption coefficient value around 46 dB/km, representing a 61.2% underestimation in the performance loss.

Furthermore, the previous model, described in [26], covers up to 450 GHz, whereas the channel loss model herein proposed covers up to 600 GHz. The same is possible thanks to the development of three additional peaks, namely, at 475 GHz, 487 GHz, and 557 GHz. This renders, for the first time to the authors' knowledge, the estimation of the molecular absorption coefficient for the Y-band (325–500 GHz). Given the large bandwidth available, THz signals can be substantially impacted by molecular absorption, while a robust channel model can be fruitful and ease that challenge regarding performance analysis.

Accordingly, the molecular absorption coefficient curves as a function of the frequency covering up to 600 GHz and for RH = 10% is plotted in Fig. 3(a). All the four models are considered for the sake of analysis consistency. It can be seen that the Full-ITU-R model does not correctly describe the peaks at 425 GHz and 487 GHz. This unconformity becomes more clear in the zoom inset from Fig. 3(a). For example, the Full-ITU-R model shows 17 dB/km at the 487 GHz peak, whereas the proposed and benchmark models suggest approximately 27 dB/km. Despite seeming relatively small the divergence, this renders a ∼63% prediction difference between the models, which can lead to misleading performance analysis. In addition, the herein developed model is easier to handle and apply rather than the Full-ITU-R model as the former only employes simple mathematical functions (such as Lorentz and Pseudo-Voigt) that can be easily simulated with very low computational complexity and computing power demand. Subsequently, the molecular absorption coefficient versus the frequency range up to 600 GHz is plotted in Fig. 3(b) for RH = 90% and for all the three pertinent models. Overall, all the three models have good agreement, showing similar performance levels from 450 GHz to 600 GHz. Despite that, one can clearly realize from the inset in Fig. 3(b) that the new proposed model (black curve) shows better agreement with a great deal of accuracy than the Full-ITU-R model (pink curve).

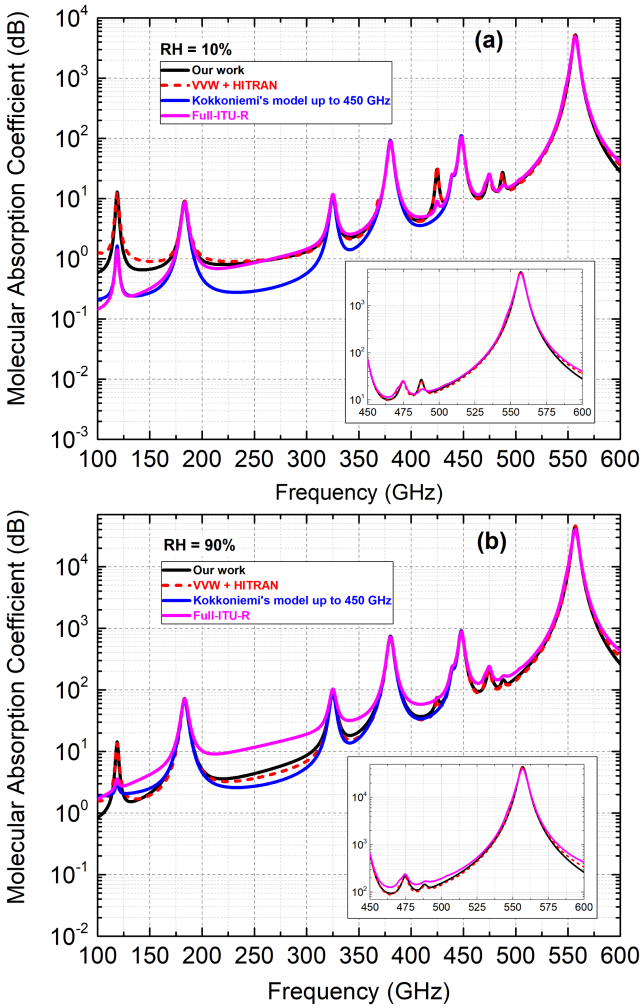

FIGURE 3. Comparison between the molecular absorption coefficient as a function of frequency from 100 to 600 GHz obtained by the different models for transmission distance of one kilometer, and different RH levels: (a) 10% and (b) 90%. In both figures: the bottom inset shows the 450 to 600 GHz band.

Next, in order to further quantify the difference among the pertinent channel models, the mean absolute error (MAE), root mean squared error (RMSE), mean absolute percentage error (MAPE), maximum absolute error (max.AE), and adjusted R-squared (adj.R^2) [42] are calculated and analyzed, assuming the VVW + HITRAN as the benchmark. Then, the MAE values are summarized in Table 1. Bear in mind that θ_{adj} was optimized to minimize the MAE for the following frequency bands: 110 to 300 GHz, 220 to 325 GHz, 275 to 450 GHz, 100 to 450 GHz, 325 to 500 GHz, 450 to 600 GHz, and 100 to 600 GHz. Hence, one must choose the desired frequency band and set θ_{adj} as indicated in Table 1 in order to reproduce the results. Then, by analyzing the MAE values (dB/km) from Table 1, one can note that the new proposed model has lower MAE's values than do the remaining models [22], [26], for all frequency bands, and considering RH ranging from 10% to 90%. For example, in the 275 to

TABLE 1. Results of the Error Metrics Used in the Evaluation of the Proposed Model for Different Frequency Bands and RH = 10%, 50% and 90%

Models	RH 10%					RH 50%					RH 90%				
	MAE (dB/km)	RMSE (dB/km)	MAPE (%)	max.AE (dB/km)	adj.R^2	MAE (dB/km)	RMSE (dB/km)	MAPE (%)	max.AE (dB/km)	adj.R^2	MAE (dB/km)	RMSE (dB/km)	MAPE (%)	max.AE (dB/km)	adj.R^2
110 to 300 GHz (G-band) @$\theta_{adj} = 1.35 \times 10^{-4}$															
Full-ITU-R	0.5951	1.489	31.76	11.560	0.3037	2.3358	2.8303	81.68	10.891	0.7788	5.7433	6.6167	135.38	12.143	0.6061
Kokkoniemi	0.9184	1.558	62.38	11.335	0.2376	0.8497	1.4706	24.57	10.719	0.9403	1.0867	1.5812	22.10	10.099	0.9775
Our work	0.1486	0.238	10.31	1.004	0.9822	0.3258	0.4220	12.53	1.359	0.9951	0.5251	0.7143	12.91	2.990	0.9954
220 to 325 GHz (H-band) @$\theta_{adj} = 9.04 \times 10^{-5}$															
Full-ITU-R	0.1356	0.1607	10.62	0.595	0.9881	3.8889	4.0197	118.77	5.923	0.6953	9.8722	10.1546	183.19	13.824	0.3863
Kokkoniemi	0.6560	0.6625	58.70	0.868	0.7969	0.9132	0.9408	28.50	1.791	0.9833	1.1724	1.2292	21.55	2.541	0.9910
Our work	0.0580	0.0781	4.64	0.344	0.9972	0.2517	0.3131	7.23	1.173	0.9982	0.4766	0.5989	7.79	1.347	0.9979
275 to 450 GHz (WRC-19) @$\theta_{adj} = 3.8 \times 10^{-6}$															
Full-ITU-R	1.0567	3.0863	12.53	25.402	0.9759	7.4241	8.0336	54.87	18.219	0.9931	18.5875	19.9406	78.63	40.147	0.9863
Kokkoniemi	1.5473	3.7354	27.96	29.570	0.9647	2.2997	4.3968	11.19	27.172	0.9979	3.6545	6.5971	9.02	28.941	0.9985
Our work	0.3187	0.6627	3.28	3.908	0.9989	1.0396	1.8796	4.02	12.067	0.9996	3.0042	4.5468	5.84	16.691	0.9993
100 to 450 GHz @$\theta_{adj} = 9.6 \times 10^{-5}$															
Full-ITU-R	0.8747	2.4496	25.26	25.395	0.9734	4.6828	5.9368	63.35	18.209	0.9933	11.6303	14.6240	99.06	40.125	0.9870
Kokkoniemi	1.2536	2.8798	45.85	29.563	0.9632	1.5496	3.2825	17.47	27.161	0.9980	2.3255	4.7961	15.19	28.932	0.9986
Our work	0.2666	0.5023	9.62	3.818	0.9989	0.8725	1.4600	13.75	11.609	0.9996	2.1145	3.5456	15.69	17.504	0.9992
325 to 500 GHz (Y-band) @$\theta_{adj} = 1.0 \times 10^{-6}$															
Full-ITU-R	1.5371	3.3427	12.78	25.402	0.9705	10.6491	11.6120	32.03	22.269	0.9851	26.6603	28.8191	44.68	52.903	0.9706
Our work	0.4879	0.8091	3.29	3.911	0.9983	1.9416	2.9585	4.00	12.080	0.9990	4.8584	6.2640	6.18	16.848	0.9986
450 to 600 GHz @$\theta_{adj} = 5.0 \times 10^{-7}$															
Full-ITU-R	26.8041	76.6931	11.23	494.546	0.9929	158.6426	434.6169	18.22	2864.266	0.9906	324.8278	861.4013	23.46	5714.104	0.9882
Our work	10.0678	23.7893	6.42	147.484	0.9993	48.2137	109.4063	6.66	672.779	0.9994	86.5294	190.1541	6.84	1142.955	0.9994
100 to 600 GHz @$\theta_{adj} = 9.6 \times 10^{-5}$															
Full-ITU-R	8.6535	42.0565	21.05	494.51	0.9935	50.8742	238.1015	49.81	2863.945	0.9914	105.5973	471.9682	76.38	5713.154	0.9893
Our work	3.2126	13.0205	8.72	147.34	0.9994	15.1124	59.8562	11.69	672.311	0.9995	27.5067	104.0468	13.10	1141.861	0.9995

max.AE = Maximum Absolute Error and adj.R^2 = adjusted R-squared.

450 GHz range, for $\theta_{adj} = 3.8 \times 10^{-6}$, our model yields a MAE of 0.32 dB/km, 1.04 dB/km, and 3 dB/km for RH = 10%, 50%, and 90%, respectively. In contrast, the previous model [26] resulted in a MAE of 1.55 dB/km, 2.3 dB/km, 3.6 dB/km for RH = 10%, 50%, and 90%, respectively. Thus, such an error difference is substantially relevant and may poorly estimate the performance analysis of THz networks. Another error metric analyzed here is the RMSE. This mechanism penalizes larger errors more than small errors. In this manner, for the 275 to 450 GHz range, and under RH = 90%, the proposed channel model suggests an RMSE of 4.5 dB/km, whereas the previous model [26] results in an RMSE of 6.6 dB/km. Hence, the latter envisages more extreme errors than the new proposed model. Afterwards, for the 100 to 450 GHz range, under the most critical condition such as RH = 90%, a MAPE around 15.7% is obtained for the proposed model. In comparison, the previous model [26], achieved a MAPE of 15.2%, which is slightly less than the MAPE of the proposed model. Still concerning the error evaluation, the max.AE and adj.R^2 metrics yield values of 17.5 dB/km and 0.9992, respectively, for the proposed channel model. In contrast, 28.9 dB/km and 0.9986 are obtained for the model in [26]. As a result, the new proposed model can be deemed as a promising tool for supporting and advancing the performance of THz networks in a more accurate way.

Next, let us consider the 450–600 GHz range, and $\theta_{adj} = 5.0 \times 10^{-7}$, then, the proposed channel model yields a MAE around 10.1 dB/km, 48.2 dB/km, and 86.5 dB/km for RH = 10%, 50%, and 90%, respectively. Nonetheless, the Full-ITU-R model obtained a MAE of 26.8 dB/km, 158.6 dB/km, and

325 dB/km for RH = 10%, 50%, and 90%, respectively. This strongly suggests that former is a more robust way for estimating the molecular absorption coefficients in this region, with a substantial MAE difference between the models, especially for RH = 90%. Additionally, under the same range and θ_{adj}, the metrics such as RMSE, MAPE, max.AE and adj.R^2 result in 190 dB/km, 6.8%, 1,143 dB/km, and 0.9994, respectively, for the new proposed model. The Full-ITU-R model whereas yields 861 dB/km, 23.5%, 5,714 dB/km, and 0.9882, respectively, for the same error metrics. All the results are summarized in Table 1. Consequently, the Full-ITU-R model clearly shows a larger discrepancy against the benchmark. Thus, the new model is a more reliable alternative for evaluating the molecular absorption coefficient under the range of 450 to 600 GHz.

1) NOVEL PROPOSED MODEL WITH REDUCED TERMS FOR THE 450–600 GHZ RANGE

The new proposed channel model, based on closed-form equations, for estimating the molecular absorption coefficient in the 100 to 600 GHz range is mainly given by (18). In order to reduce the number of equations to describe only the 450 to 600 GHz band, which was never addressed before in the literature, the new model with reduced terms is herein developed. Accordingly, the reduced absorption coefficient can be expressed as

$$k_a^{red}(f) = \sum_{j=6}^{10} y_j(f,\mu) + g(f,\mu), \tag{59}$$

where $y_6(f,\mu)$ to $y_{10}(f,\mu)$, and $g(f,\mu)$ are given by (24) to (28), and (56), respectively.

In order to assess the performance of the new model with reduced terms (y_6 to y_{10}), we compare the former with its own complete version with all terms (y_1 to y_{10}) and also against the benchmark model (VVW + HITRAN), under the range 450 to 600 GHz, and for RH = 90%. Then, the molecular absorption coefficient versus the frequency range (450–600 GHz) in plotted in Fig. 4. In addition, also shown in Fig. 4 is the results for the difference among the complete proposed model will all terms, the reduced proposed model, and finally the benchmark (VVW + HITRAN). Overall, it can be observed from Fig. 4 an excellent agreement between the proposed model and benchmark, showing complete convergence up to 580 GHz. In addition, it can be seen from Fig. 4 that in the 450 to 500 GHz range, the proposed model with reduced terms (green dashed curve) has slightly better performance than do the complete model with all terms (pink curve). However, both models yield virtually the same performance for the 500–600 GHz range. The results for different error metrics are summarized in Table 2.

Moreover, the error metrics for the new developed models with all terms as well as reduced terms compared against the benchmark in the 450 to 600 GHz range for RH = 10% and 90%, is summarized in Table 2. Bear in mind that $g(f,\mu)$ remains the same for both models, but $\theta_{adj} = 5 \times 10^{-7}$ for the complete model with all terms, and $\theta_{adj} = 3.05 \times 10^{-3}$ for the reduced terms model. One can realize that the error metrics are similar for both complete and reduced terms models. Besides that, only a small reduction in terms of MAE and MAPE can be seen for the reduced terms model in Table 2, which is owing to the optimization of θ_{adj}. As a conclusion, both complete and reduced terms models are accurate, predicting with success the actual absorption losses. The experimental validation of the total atmospheric absorption coefficient is carried out in the next Section.

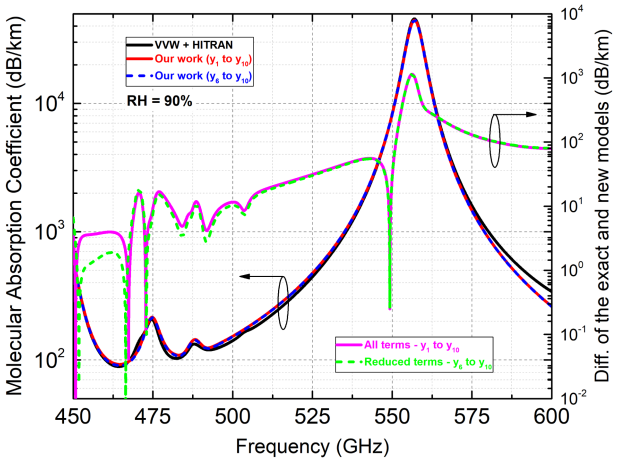

FIGURE 4. Left y-axis: comparison between the molecular absorption coefficient curves given by the proposed model with all terms (y_1 to y_{10}), reduced terms (y_6 to y_{10}), and the exact model as a function of frequency for the 450 to 600 GHz band, for a temperature of 298 K and RH = 90%. Right y-axis: comparison between the differences of the proposed models with all terms and reduced terms relative to the exact model.

TABLE 2. Results of the Error Metrics Used to Evaluate the Proposed Models With All Terms and Reduced Terms Relative to the Exact Model for the 450 to 600 GHz Band and for RH = 10% and 90%

450 to 600 GHz					
RH = 10%					
Models	**MAE (dB/km)**	**RMSE (dB/km)**	**MAPE (%)**	**max.AE (dB/km)**	**adj.R^2**
All terms (y_1 to y_{10}) $\theta_{adj} = 5 \times 10^{-7}$	10.07	23.79	6.42	147.48	0.99932
Red. terms (y_6 to y_{10}) $\theta_{adj} = 3.05 \times 10^{-3}$	10.05	23.89	6.14	147.81	0.99931
RH = 90%					
Models	**MAE (dB/km)**	**RMSE (dB/km)**	**MAPE (%)**	**max.AE (dB/km)**	**adj.R^2**
All terms (y_1 to y_{10}) $\theta_{adj} = 5 \times 10^{-7}$	86.53	190.15	6.84	1142.96	0.9994
Red. terms (y_6 to y_{10}) $\theta_{adj} = 3.05 \times 10^{-3}$	86.06	190.45	6.43	1143.91	0.9994

max.AE = Maximum Absolute Error and adj.R^2 = adjusted R-squared.

B. EXPERIMENTAL VALIDATION OF THE TOTAL ATMOSPHERIC ABSORPTION COEFFICIENT

The total atmospheric absorption coefficient is defined as the sum of the molecular absorption coefficient, $k_a(f)$ given by

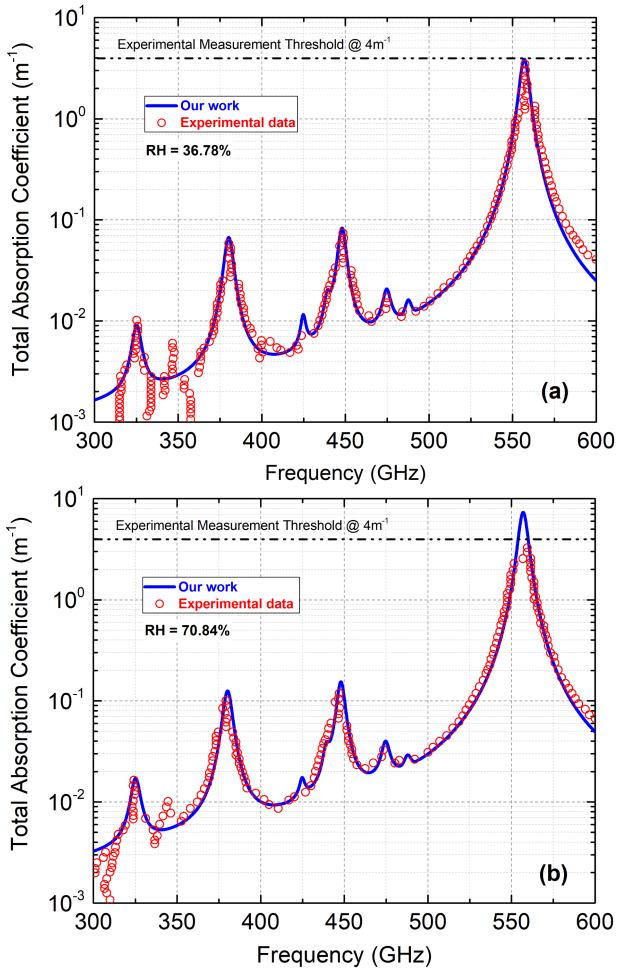

FIGURE 5. Comparison between the proposed model curve and experimental data [29] of the total atmospheric absorption coefficients in the 300 to 600 GHz range for: (a) RH = 36.78%, and (b) RH = 70.84%. The lack of experimental data above the threshold (4 m $^{-1}$) is due to saturation effects in the measurement.

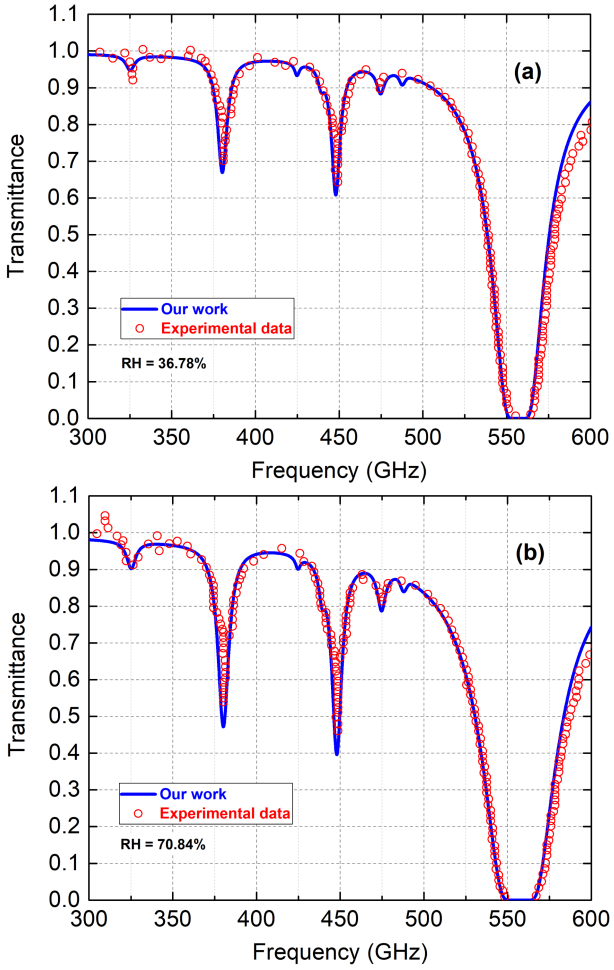

FIGURE 6. Comparison between the proposed model curve and experimental data [29] of the atmospheric transmittance in the 300 to 600 GHz range for: (a) RH = 36.78%, and (b) RH = 70.84%.

(18), and the water vapor continuum absorption coefficient, $k_c(f)$, given by (57). Then, let us analyse $k_c(f)$ and the experimental data [29] used here for validation purposes of the new developed formalism model.

The total absorption coefficient was measured using FTIR (Fourier transform infrared spectrometer) for room temperature [29]. The measurements were performed for the frequency range of 300 GHz to 1.5 THz, varying the amount of water vapor (RH) in a chamber for different transmission paths. To calculate the contribution of $k_c(f)$ to the total absorption coefficient, (57) is used, whose $C_W = 4.39 \times 10^{-8}$ (dB/km)/(hPa GHz)^2 and $C_A = 4 \times 10^{-9}$ (dB/km)/(hPa GHz)^2 [32].

Accordingly, adding $k_c(f)$ to $k_a(f)$ results in the total absorption coefficient, whose performance versus the frequency range from 300 to 600 GHz are show in Fig. 5, for RH = 36.78% (Fig. 5(a)) and for RH = 70.84% (Fig. 5(b)). The experimental data of the total absorption coefficient, which can be found in [29], is also plotted in Fig. 5, considering RH = 36.78% and RH = 70.84% for the same frequency range. Further, in Fig. 5(a) and (b) dash-dot lines indicating the experimental measurement threshold for $k = 4$ m^{-1} are shown. This limitation is due to saturation effects of the measurement equipment in [29]. The average errors of measurement for RH = 36.78% and RH = 70.84% are 4% and 2.87%, respectively [29]. Remarkably, both experimental data and new developed model show very good overall agreement, suggesting a great deal of accuracy. One can clearly realize from Fig. 5 that the new proposed model shows convergence with the experimental data.

Additionally, the simulated atmospheric transmittance was calculated by (9), which depends on the total absorption coefficient, $k(f) = k_a(f) + k_c(f)$, where $k_a(f)$ is given by (18) and $k_c(f)$ given (57). Then, the transmittance performance considering a 6-meter transmission path for RH = 36.78% and 70.84% are illustrated in Fig. 6(a) and (b), respectively. Those conditions were used in the measurement of the experimental data analysis of the transmittance in [29]. Hence, the experimental transmittance versus the frequency range 300 to 600 GHz is also plotted in Fig. 6. Once again, the channel

TABLE 3. Comparison of the Link Budget for Different Channels and a Fixed Distance Obtained by the Proposed Model and the Benchmark Model

Parameters	Models					
	VVW + HITRAN	Our work	VVW + HITRAN	Our work	VVW + HITRAN	Our work
f_c (GHz)	157.75		261.36		317.52	
Δf (GHz)	12.5		17.28		8.64	
θ_{adj}	1.9×10^{-4}		9.04×10^{-5}		9.04×10^{-5}	
k_a (m^{-1})	3.51×10^{-4}	3.55×10^{-4}	5.2×10^{-4}	4.97×10^{-4}	2.29×10^{-3}	2.32×10^{-3}
k_c (m^{-1})	3.73×10^{-4}		1.02×10^{-3}		1.51×10^{-3}	
k (m^{-1})	7.24×10^{-4}	7.28×10^{-4}	1.54×10^{-3}	1.52×10^{-3}	3.8×10^{-3}	3.83×10^{-3}
k (dB/km)	3.14	3.16	6.69	6.60	16.5	16.6
RE (%)†	–	0.55	–	1.3	–	1.29
$G_{Tx/Rx}$ (dBi)	49.9		54.2		55.9	
d (m)	1000		1000		1000	
P_n (dBm)	-63.1	-63.1	-61.6	-61.6	-64.53	-64.53
PL (dB)	139.6	139.6	147.5	147.48	159.0	159.12
P_{Rx} (dBm)	-39.8	-39.8	-39.0	-39.0	-47.11	-47.24
SNR (dB)	23.3	23.3	22.6	22.6	17.4	17.3
BER	1.3×10^{-13}	1.3×10^{-13}	7.7×10^{-12}	7.7×10^{-12}	1.0×10^{-4}	1.2×10^{-4}

†RE = relative error between the benchmark model (VVW + HITRAN) and the proposed model.

model converges towards the experimental data correctly predicting the atmospheric transmittance.

C. LINK BUDGET CALCULATIONS CONSIDERING THE TOTAL ATMOSPHERIC ABSORPTION COEFFICIENT

In this section, link budget calculations are carried out in order to employ the new proposed model for performance analysis of THz networks from 100–600 GHz. The goal is to show that the new developed tool is simpler and faster to implement than numerical models like the VVW + HITRAN model.

Accordingly, the developed tool can be used to evaluate different THz scenarios with line-of-sight supporting several applications as illustrated in Fig. 1. In this way, the performance evaluation is done by means of link budget calculations, which estimates the power at the receiver and many other quantities related with gains and losses in the link. Then, the SNR and BER are considered and calculated for different THz links.

To do so, let us consider the antenna gain of the LOS THz link as follows [26]

$$G_{Tx/Rx} = 20 \log_{10} \left(\frac{\sqrt{A_e} \pi d_{ant} f}{c} \right), \tag{60}$$

given in dBi, A_e is the aperture efficiency and d_{ant} is the diameter of the parabolic reflector antenna. The calculations are performed considering $A_e = 0.7$ and $d_{ant} = 225$ mm, which are the values given by [26]. Then, the link center frequencies (f_c) are: 157.75, 261.36, 317.52, 410, 484 and 542 GHz. The respective available bandwidths (Δf) are: 12.5, 17.28, 8.64, 18.5, 6.5 and 25.9 GHz. The first center frequency and available bandwidth are defined in [43], the second and third are given by [14], the fourth, fifth and sixth are taken from [33], [44], for the sake of analysis consistency.

Accordingly, the atmospheric conditions for the THz channels considered are $T = 296$ K, $p = 1$ atm and RH $= 50\%$. Next, the molecular and water vapor continuum absorption coefficients are obtained via (18) and (57), respectively. Thus the atmospheric absorption coefficient is given by the sum of (18) and (57). The optimization parameters θ_{adj} used in the calculation of the molecular absorption coefficient are provided in Tables 3 and 4, considering their respective frequency bands. Thus, the transmitter power and noise figure considered in the evaluation are $P_{Tx} = 0$ dBm and $NF = 10$ dB, respectively [45], [46], [47], [48], [49]. Subsequently, the P_n, P_{Rx}, PL, SNR and BER of the THz link are determined by (5), (9), (11), (12) and (13), respectively. The results obtained are shown in Tables 3 and 4. The THz link distances are always 1 km in Table 3, but they are different in Table 4 so that the remaining parameters/metrics such as SNR and BER can be further stressed. The comparison of the proposed model against the benchmark (VWW + HITRAN) in terms of several link budget parameters including key figure-of-merits such as the PL, SNR, and BER for a fixed distance ($d = 1000$ m) are summarized in Table 3. Noteworthy, the relative errors between the models are indeed small and can even be considered negligible. For example, as can be seen in Table 3, for $f_c = 157.75$ GHz, $RE = 0.55\%$ only. Once again, the proposed model converges towards the benchmark. This is important as the remaining parameters/metrics are also impacted, but as shown in Table 3, the PL, SNR, and BER basically show the same performance for both models. In this manner, for both model and benchmark, the PL, SNR, and BER are 139.6 dB, 23.3 dB, and 1.3×10^{-13}, respectively, considering $f_c = 157.75$ GHz. Likewise, the same analysis holds valid if one considers $f_c = 261.36$ GHz. Interestingly, one can note that the SNR for these two THz link scenarios ($f_c = 157.75$ GHz and $f_c = 261.36$ GHz) is high enough to yield a BER level under the regime of error-free data transmissions. Eventually, this can enable different network scenarios and consequently support many broadband applications.

Lastly, a similar link budget analysis is carried out but for THz links at higher frequencies such as $f_c = 410$ GHz, $f_c = 484$ GHz, and $f_c = 542$ GHz, as summarized in Table 4. Bear

TABLE 4. Comparison of the Link Budget for Different Channels and Distances Obtained by the Proposed Model and the Benchmark Model

Parameters	Models					
	VVW + HITRAN	Our work	VVW + HITRAN	Our work	VVW + HITRAN	Our work
f_c (GHz)	410		484		542	
Δf (GHz)	18.5		6.5		25.9	
θ_{adj}	1×10^{-6}		1×10^{-6}		5×10^{-7}	
k_a (m^{-1})	3.73×10^{-3}	3.86×10^{-3}	1.21×10^{-2}	1.24×10^{-2}	2.27×10^{-1}	2.3×10^{-1}
k_c (m^{-1})	2.52×10^{-3}		3.51×10^{-3}		4.40×10^{-3}	
k (m^{-1})	6.25×10^{-3}	6.38×10^{-3}	1.56×10^{-2}	1.59×10^{-2}	2.31×10^{-1}	2.34×10^{-1}
k (dB/km)	27.14	27.7	67.8	69.1	1005	1018
RE (%)†	–	2.04	–	1.89	–	1.28
$G_{Tx/Rx}$ (dBi)	58.2		59.6		60.6	
d (m)	700		400		45	
P_n (dBm)	-61.22	-61.22	-65.76	-65.76	-59.8	-59.8
PL (dB)	160.61	161	165.3	165.8	165.4	166
P_{Rx} (dBm)	-44.68	-44.69	-46.11	-46.6	-44.3	-44.8
SNR (dB)	16.54	16.53	19.6	19.2	15.5	15.0
BER	3.9×10^{-4}	4.0×10^{-4}	1.0×10^{-6}	2.6×10^{-6}	1.4×10^{-3}	2.5×10^{-3}

†RE = relative error between the benchmark model (VVW + HITRAN) and the proposed model.

in mind that the THz link distances are different for each center frequency. Once more, even under different link distances, the relative error between the model and benchmark is small in general, which yields virtually similar levels of the key figure-of-merits, i.e., the SNR and BER. Remarkably, it can be seen in Table 4 that for $f_c = 542$ GHz, the SNR ($\sim$15 dB) and BER ($\sim 2 \times 10^{-3}$) resulted in poor levels, which hinders the performance of such THz link. Thus, it can be concluded that the new channel model is robust and proved to be a useful tool for performance evaluation of THz networks.

IV. CONCLUSION

In this article, a novel mathematical formalism rendering completely accuracy for performance analysis of line-of-sight THz networks within the frequency range of 100–600 GHz was proposed. The new developed channel model takes into account both the water vapor continuum absorption loss and the molecular absorption loss. In addition, the model's formalism in based on closed-form absorption line shape equations and a fitting parameter (equalization factor), developed to accurately match the channel response given by the HITRAN spectroscopic database. The latter is considered as a benchmark, against which the performance can be compared. Moreover, several error metrics (such as MAE, RMSE, and MAPE) have been considered and analyzed. The new channel model was validated and compared against many different models. It was shown that the channel model accurately reproduces the experimental dataset HITRAN, which is considered the benchmark. In other words, the model shown complete convergence and is a more appropriate and accurate choice for performance assessment of THz networks due to its simplicity. Its great performance indicator sets a new benchmark for analytical performance evaluation of such networks. This new channel model can be successfully applied for accurate performance evaluation of THz networks within a large frequency range, including the prominent D-band. Moreover, the model can be further applied for evaluating the link transmission distance of THz networks and their performance in terms of key figures-of-merit such as SNR and BER. Therefore, this robust and easy-to-use channel loss model is deemed as a unique tool and a new benchmark to be added to the portfolio for the performance evaluation of THz networks.

REFERENCES

[1] M. Z. Chowdhury, M. Shahjalal, S. Ahmed, and Y. M. Jang, "6G wireless communication systems: Applications, requirements, technologies, challenges, and research directions," *IEEE Open J. Commun. Soc.*, vol. 1, pp. 957–975, 2020, doi: 10.1109/OJCOMS.2020.3010270.

[2] H. Tataria, M. Shafi, A. F. Molisch, M. Dohler, H. Sjöland, and F. Tufvesson, "6G wireless systems: Vision, requirements, challenges, insights, and opportunities," in *Proc. IEEE*, vol. 109, no. 7, pp. 1166–1199, Jul. 2021, doi: 10.1109/JPROC.2021.3061701.

[3] S. Carson and S. Davies, "Ericsson mobility report," Ericsson, Stockholm, Sweden, Rep. no. EAB-22:010742 Uen Rev D., Nov. 2022.

[4] O. Hashash, C. Chaccour, W. Saad, T. Yu, K. Sakaguchi, and M. Debbah, "The seven worlds and experiences of the wireless metaverse: Challenges and opportunities," 2023. [Online]. Available: https://arxiv.org/abs/2304.10282

[5] L. U. Khan, M. Guizani, D. Niyato, A. Al-Fuqaha, and M. Debbah, "Metaverse for wireless systems: Architecture, advances, standardization, and open challenges," 2023. [Online]. Available: https://arxiv.org/abs/2301.11441

[6] D. Neves et al., "Beyond 5G fronthaul based on FSO using spread spectrum codes and graphene modulators," *Sensors*, vol. 23, no. 8, Apr. 2023, Art. no. 3791, doi: 10.3390/s23083791.

[7] I. F. Akyildiz, A. Kak, and S. Nie, "6G and beyond: The future of wireless communications systems," *IEEE Access*, vol. 8, pp. 133995–134030, 2020, doi: 10.1109/ACCESS.2020.3010896.

[8] T. R. Raddo et al., "Transition technologies towards 6G networks," *EURASIP J. Wireless Commun. Netw.*, vol. 2021, Apr. 2021, Art. no. 100, doi: 10.1186/s13638-021-01973-9.

[9] J. He, K. Yang, and H. H. Chen, "6G cellular networks and connected autonomous vehicles," *IEEE Netw.*, vol. 35, no. 4, pp. 255–261, Jul./Aug. 2021, doi: 10.1109/MNET.011.2000541.

[10] M. Noor-A-Rahim et al., "6G for vehicle-to-everything (V2X) communications: Enabling technologies, challenges, and opportunities," *Proc. IEEE*, vol. 110, no. no. 6, pp. 712–734, Jun. 2022, doi: 10.1109/JPROC.2022.3173031.

[11] L. Bariah and M. Debbah, "The interplay of AI and digital twin: Bridging the gap between data driven and model-driven approaches," 2023. [Online]. Available: https://arxiv.org/abs/2209.12423

[12] I. F. Akyildiz and H. Guo, "Holographic-type communication: A new challenge for the next decade," *ITU J. Future Evolving Technol.*, vol. 3, no. 2, pp. 421–442, Sep. 2022, doi: 10.52953/YRLL3571.

[13] V. Petrov, T. Kürner, and I. Hosako, "IEEE 802.15.3 d: First standardization efforts for sub-terahertz band communications toward 6G," *IEEE Commun. Mag.*, vol. 58, no. 11, pp. 28–33, Nov. 2020, doi: 10.1109/MCOM.001.2000273.

[14] *IEEE Standard for High Data Rate Wireless Multi-Media Networks–Amendment 2: 100 Gb/s Wireless Switched Point-to-Point Physical Layer*, IEEE Standard 802.15.3d-2017 (Amendment to IEEE Standard 802.15.3-2016 as amended by IEEE Standard 802.15.3e-2017), Oct. 2017, pp. 1–55, doi: 10.1109/IEEESTD.2017.8066476.

[15] T. Kürner, "THz communications–a candidate for a 6G radio?," in *Proc. 22nd Int. Symp. Wireless Pers. Multimedia Commun.*, Lisbon, Portugal, 2019, pp. 1–5, doi: 10.24355/dbbs.084-202008031406-0.

[16] T. Kürner and A. Hirata, "On the impact of the results of WRC 2019 on THz communications," in *Proc. 3rd Int. Workshop Mobile Terahertz Syst.*, Essen, Germany, 2020, pp. 1–3, doi: 10.1109/IWMTS49292.2020.9166206.

[17] D. Serghiou, M. Khalily, T. Brown, and R. Tafazolli, "Terahertz channel propagation phenomena, measurement techniques and modeling for 6G wireless communication applications: A survey, open challenges and future research directions," *IEEE Commun. Surv. Tut.*, vol. 24, no. 4, pp. 1957–1996, Fourth Quarter. 2022, doi: 10.1109/COMST.2022.3205505.

[18] J. M. Jornet and I. F. Akyildiz, "Channel modeling and capacity analysis for electromagnetic wireless nanonetworks in the Terahertz band," *IEEE Trans. Wireless*, vol. 10, no. 10, pp. 3211–3221, Oct. 2011, doi: 10.1109/TWC.2011.081011.100545.

[19] P. W. Rosenkranz, "Water vapor microwave continuum absorption: A comparison of measurements and models," *Radio Sci.*, vol. 33, no. 4, pp. 919–928, Jul./Aug. 1998, doi: 10.1029/98RS01182.

[20] J. H. V. Vleck and V. F. Weisskopf, "On the shape of collision-broadened lines," *Rev. Modern Phys.*, vol. 17, no. 2–3, pp. 227–236, Apr. 1945, doi: 10.1103/RevModPhys.17.227.

[21] I. E. Gordon, "The HITRAN2020 molecular spectroscopic database," *J. Quantitative Spectrosc. Radiative Transfer*, vol. 277, Jan. 2022, Art. no. 107949, doi: 10.1016/j.jqsrt.2021.107949.

[22] ITU-R, "Attenuation by atmospheric gases and related effects," Report ITU-R P.676-13, Aug. 2022. [Online]. Available: https://www.itu.int/rec/R-REC-P.676

[23] ITU-R, "Attenuation by atmospheric gases and related effects," Report ITU-RP.676-10, Sep. 2013. [Online]. Available: https://www.itu.int/rec/R-REC-P.676

[24] J. Kokkoniemi, J. Lehtomäki, and M. Juntti, "Simplified molecular absorption loss model for 275–400 gigahertz frequency band," in *Proc. 12th Eur. Conf. Antennas Propag.*, London, U.K., 2018, pp. 1–5, doi: 10.1049/cp.2018.0446.

[25] J. Kokkoniemi, J. Lehtomäki, and M. Juntti, "Simple molecular absorption loss model for 200–450 gigahertz frequency band," in *Proc. Eur. Conf. Netw. Commun.*, Valencia, Spain, 2019, pp. 219–223, doi: 10.1109/EuCNC.2019.8801950.

[26] J. Kokkoniemi, J. Lehtomäki, and M. Juntti, "A line-of-sight channel model for the 100–450 gigahertz frequency band," *EURASIP J. Wireless Commun. Netw.*, vol. 2021, 2021, Art. no. 88, doi: 10.1186/s13638-021-01974-8.

[27] H. J. Liebe, "An updated model for millimeter wave propagation in moist air," *Radio Sci.*, vol. 20, no. 5, pp. 1069–1089, Sep./Oct. 1985, doi: 10.1029/RS020i005p01069.

[28] C. J. Gibbins, "Improved algorithms for the determination of specific attenuation at sea level by dry air and water vapor, in the frequency range 1-350 GHz," *Radio Sci.*, vol. 21, no. 6, pp. 949–954, Nov./Dec. 1986, doi: 10.1029/RS021i006p00949.

[29] D. M. Slocum, E. J. Slingerland, R. H. Giles, and T. M. Goyette, "Atmospheric absorption of terahertz radiation and water vapor continuum effects," *J. Quantitative Spectrosc. Radiative Transfer*, vol. 127, pp. 49–63, Sep. 2013, doi: 10.1016/j.jqsrt.2013.04.022.

[30] D. M. Slocum, T. M. Goyette, E. J. Slingerland, R. H. Giles, and W. E. Nixon, "Terahertz atmospheric attenuation and continuum effects," *Proc. SPIE*, vol. 8716, pp. 24–37, 2013, doi: 10.1117/12.2015471.

[31] Y. Yang, M. Mandehgar, and D. Grischkowsky, "Determination of the water vapor continuum absorption by THz-TDS and molecular response theory," *Opt. Exp.*, vol. 22, no. 4, pp. 4388–4403, Feb. 2014, doi: 10.1364/OE.22.004388.

[32] J. Kwon, M. Park, and T. Jeon, "Determination of the water vapor continuum absorption by THz pulse transmission using long-range multipass cell," *J. Quantitative Spectrosc. Radiative Transfer*, vol. 272, 2021, Art. no. 107811, doi: 10.1016/j.jqsrt.2021.107811.

[33] T. Schneider, A. Wiatrek, S. Preussler, M. Grigat, and R. P. Braun, "Link budget analysis for terahertz fixed wireless links," *IEEE Trans. Terahertz Sci. Technol.*, vol. 2, no. 2, pp. 250–256, Mar. 2012, doi: 10.1109/TTHZ.2011.2182118.

[34] T. S. Rappaport et al., "Wireless communications and applications above 100 GHz: Opportunities and challenges for 6G and beyond," *IEEE Access*, vol. 7, pp. 78729–78757, 2019, doi: 10.1109/ACCESS.2019.2921522.

[35] M. Taherkhani, Z. G. Kashani, and R. Sadeghzadeh, "Average bit error rate and channel capacity of terahertz wireless line-of-sight links with pointing errors under combined effects of turbulence and snow," *Appl. Opt.*, vol. 59, no. 33, pp. 10345–10356, Nov. 2020, doi: 10.1364/AO.403390.

[36] S. Liu, X. Yu, R. Guo, Y. Tang, and Z. Zhao, "THz channel modeling: Consolidating the road to THz communications," *China Commun.*, vol. 18, no. 5, pp. 33–49, May 2021, doi: 10.23919/JCC.2021.05.003.

[37] W. Lee et al., "Coherent terahertz wireless communication using dual-parallel MZM-based silicon photonic integrated circuits," *Opt. Exp.*, vol. 30, no. 2, pp. 2547–2563, Jan. 2022, doi: 10.1364/OE.446516.

[38] R. Nobrega, A. Sanches, M. Loiola, A. Jurado-Navas, W. Gerstacker, and T. Raddo, "Performance evaluation of nano-RTD VCO devices for on-body THz nano-communication applications," in *Proc. 47th Int. Conf. Infrared Millimeter Terahertz Waves*, Delft, Netherlands, 2022, pp. 1–2, doi: 10.1109/IRMMW-THz50927.2022.9895553.

[39] G. L. Bastin et al., "Measurements of aperture averaging on bit-error-rate," in *Proc. SPIE*, vol. 5891, 2005, Art. no. 589102, doi: 10.1117/12.619459.

[40] S. Paine, "The am atmospheric model," Smithsonian Astrophysical Observatory: Cambridge, MA, USA, Tech. Rep. 152, Jul. 2022, doi: 10.5281/zenodo.6774378.

[41] T. Ida, M. Ando, and H. Toraya, "Extended pseudo-Voigt function for approximating the Voigt profile," *J. Appl. Crystallogr.*, vol. 33, pp. 1311–1316, 2000, doi: 10.1107/S0021889800010219.

[42] D. Chicco, M. Warrens, and G. Jurman, "The coefficient of determination R-squared is more informative than SMAPE, MAE, MAPE, MSE and RMSE in regression analysis evaluation," *PeerJ Comput. Sci.*, vol. 7, 2021, Art. no. e623, doi: 10.7717/peerj-cs.623.

[43] ECC Recommendation (18)01, "Radio frequency channel/block arrangements for fixed service systems operating in the bands 130–134 GHz, 141–148.5 GHz, 151.5–164 GHz and 167–174.8 GHz," Apr. 2018. [Online]. Available: https://docdb.cept.org/document/2012

[44] K. Ishigaki, M. Shiraishi, S. Suzuki, M. Asada, N. Nishiyama, and S. Arai, "Direct intensity modulation and wireless data transmission characteristics of terahertz-oscillating resonant tunnelling diodes," *Electron. Lett.*, vol. 48, no. 10, pp. 582–583, May 2012, doi: 10.1049/el.2012.0849.

[45] H. Wang et al., "Power amplifiers performance survey 2000-Present," Aug. 2021. [Online]. Available: https://gems.ece.gatech.edu/PA_survey.html

[46] T. Chi, J. Luo, S. Hu, and H. Wang, "A multi-phase sub-harmonic injection locking technique for bandwidth extension in silicon-based THz signal generation," *IEEE J. Solid-State Circuits*, vol. 50, no. 8, pp. 1861–1873, Aug. 2015, doi: 10.1109/JSSC.2015.2422074.

[47] K. Guo and P. Reynaert, "A 0.59 THz beam-steerable coherent radiator array with 1 mW radiated power and 24.1 dBm EIRP in 40 nm CMOS," in *Proc. IEEE Int. Solid-State Circuits Conf.*, San Francisco, California, USA, 2020, pp. 442–444, doi: 10.1109/ISSCC19947.2020.9063139.

[48] D. Moro-Melgar, O. Cojocari, and I. Oprea, "High power high efficiency 475–520 GHz source based on discrete Schottky diodes," in *Proc. 50th Eur. Microw. Conf.*, Utrecht, Netherlands, 2021, pp. 607–610, doi: 10.23919/EuMC48046.2021.9338081.

[49] Z. Peng, J. Chen, H. Wang, L. Zhang, W. Hong, and X. Liu, "A 300 GHz push-push coupling VCO employing T-embedded network in CMOS technology," *IEEE Trans. Terahertz Sci. Technol.*, vol. 12, no. 4, pp. 426–429, Jul. 2022, doi: 10.1109/TTHZ.2022.3173181.

RAFAEL V. T. DA NOBREGA received the B.S. degree in physics from the Federal University of Sao Carlos (UFSCar), Brazil, in 2008, and the M.Sc. degree in electrical engineering from the University of Sao Paulo (EESC-USP), Brazil, in 2010. He is currently working toward the Ph.D. degree with the Federal University of ABC (UFABC), Brazil. He is currently an Adjunct Professor with the Federal Institute of Minas Gerais (IFMG), Formiga, Brazil. His research interests include resonant tunneling diodes and quantum devices, generation and transmission of THz waves, THz channel modeling, and 6G systems.

THIAGO R. RADDO received the M.Sc. degree in electrical engineering from the University of Sao Paulo, Sao Carlos, Brazil, in 2012, and the Ph.D. degree in engineering sciences from the Vrije Universiteit Brussel, Brussels, Belgium, in 2017. He was a Visiting Researcher at the Technical University of Denmark, Denmark, in 2013. He was affiliated with the Electrical Engineering Faculty and with the Institute for Photonics Integration, Eindhoven University of Technology, Eindhoven, The Netherlands, where he contributed to multiple European research projects including 5G-PHOS, 5G-MOBIX, CONCORDA, and QKD, in 2018. He was a Visiting Scholar at the Federal University of ABC, Brazil, in 2021. He is currently a Visiting Research Fellow with the University of Malaga, Malaga, Spain. Dr. Raddo has also been a Consultant to the world's largest ICT companies for the last four years. He has coauthored more than 65 technical publications, contributed to the technical program of international conferences, and is a member of OPTICA. His main research interests incude 6G, THz, AI, photonic integrated circuits, free-space optics, and quantum communication.

ANTONIO JURADO-NAVAS received the Ph.D. degree in telecommunication engineering from the University of Malaga, Malaga, Spain, in 2009. From 2002 to 2004, he was a Consultant at Vodafone-Spain. From 2009 to 2011, he was at the Department of Communications Engineering (Ingenieria de Comunicaciones), University of Malaga as a Postdoctoral Researcher. In 2011, he became an Assistant Professor in the same department. From 2012 to 2015, he was at Ericsson, Stockholm, Sweden, where he was working on geolocation tools for mobile networks. From 2015 to 2017, he was a Marie-Curie Fellow at the Technical University of Denmark, Denmark. In 2017, he joined Technical University of Eindhoven to work for the Electro-Optical Communications Group as an Invited Researcher. Since 2018, he has been an Associate Professor with the Communication Engineering Department, Universidad de Malaga. He is currently the Vice-Dean for Students and Professional Development with the Telecommunications Engineering School, Universidad de Malaga. His research interests include communication theory and wireless communications: free-space optical and satellite communications, terahertz systems, stochastic processes, wireless channel modeling, OCDMA, physical layer security, semantic communications, and efficient transmission techniques. He was the recipient of a Spanish Ministry of Education and Science Scholarship (2004–2008).

MURILO B. LOIOLA received the B.S., M.Sc., and Ph.D. degrees in electrical engineering from the University of Campinas (UNICAMP), Brazil, in 2002, 2005 and 2009, respectively. He was a Visiting Researcher at Access Signal Processing Lab, Ericsson AB, Sweden, in 2006, and at Ecole Normale Superieure de Cachan, France, in 2014. Since 2010, he has been with the Federal University of ABC (UFABC), Brazil, where he currently is an Associate Professor. His main research interests include wireless communications, statistical and adaptive signal processing, physical layer security, and machine learning.

ANDERSON L. SANCHES received the M.Sc. and Ph.D. degrees in electrical engineering with emphasis on telecommunication from the Sao Carlos School of Engineering, University of Sao Paulo (EESC-USP), Brazil, in 2010 and 2015, respectively. From 2019 to 2020, he was a Postdoctoral Researcher in broadband communication systems at the Department of Electronic and Electrical Engineering, University of Strathclyde, Glasgow, U.K. Since 2016, he has been an Associate Professor with the Center for Engineering, Modeling and Applied Social Sciences, Federal University of ABC (UFABC), Brazil. His research interests include modeling and performance evaluation of next-generation passive optical communications systems, advanced modulation formats, OCDMA, OFDMA, and photonic technologies towards enabling terahertz wireless systems for 6G mobile networks.

MEROUANE DEBBAH (Fellow, IEEE) is currently a Researcher, Educator, and Technology Entrepreneur. Over his career, he has founded several public and industrial research centers, start-ups and is currently a Professor with the Khalifa University of Science and Technology, Abu Dhabi, UAE, and founding Director of the 6G Center. He is a frequent keynote Speaker with international events in the field of telecommunication and AI. His research interests include interface of fundamental mathematics, algorithms, statistics, information, and communication sciences with a special focus on random matrix theory and learning algorithms. In the communication field, he has been with the heart of the development of small cells (4G), Massive MIMO (5G), and Large Intelligent Surfaces (6G) technologies. In the AI field, he is known for his work on large language models, distributed AI systems for networks, and semantic communications. He was the recipient of multiple prestigious distinctions, prizes and best paper awards (more than 35 best paper awards) for his contributions to both fields and according to research.com is ranked as the best scientist in France in the field of Electronics and Electrical Engineering. He is a WWRF Fellow, a Eurasip Fellow, an AAIA Fellow, an Institut Louis Bachelier Fellow, and a Membre émérite SEE.